Available online at www.sciencedirect.com
SCIENCE DIRECT®
Journal of Power Sources 118 (2003) 367–374
JOURNAL OF POWER SOURCES
www.elsevier.com/locate/jpowsour

Thermal modeling of a small anode supported solid oxide fuel cell

D. Larrain*, J. Van herle, F. Maréchal, D. Favrat

Laboratory for Industrial Energy Systems (LENI), Faculty of Engineering, Swiss Federal Institute of Technology, 1015 Lausanne, Switzerland

Abstract

A combined thermal and simple kinetic model is applied to a small single solid oxide fuel cell (SOFC, 20 cm^2 square cell of anode supported electrolyte with 1 cm^2 active area). The aim was to compute the temperature field to analyze the operating conditions of the active area of the cell. The cell is simulated in the conditions used for electrochemical characterization, i.e. at negligible fuel utilization and thermally non-adiabatic.

Though using a very simple kinetic model, the simulated polarization curves fit the experimental results at high current density where the curve slope tends to decrease. The simulated temperature field shows clearly that this aspect of the curve is explained by a local temperature increase (of 30 K at 1 A/cm^2). The temperature of the active area can be plotted versus the current and this result fits previous measurements.

Finally, the temperature profile simulated shows that, with the usual temperature measurement used in standard electrochemical testing, a few millimeters away from the active surface, does not detect the effective cell temperature. In a stack modeling perspective, the quality of the kinetic model used is essential. This model, combined with a parameter estimation tool, allows using experimental results to end, from routine measurements, with an accurate and up-to-date kinetic model.

Keywords: Solid oxide fuel cell; Model; Kinetics; Local heating

1. Introduction

In operation, the temperature field in a solid oxide fuel cell (SOFC) stack can show gradients up to 100 K [1–3]. As the electrochemical reactions are activated with temperature, a non-homogeneous current density field is caused by fuel and air utilization and local temperature increase. Kinetics of the electrochemical reaction need a special focus as they are responsible both for the power output and the heat sources of the stack. Reports are published on SOFC electrode kinetics treating in detail the reaction path [4,5], microstructure of the anode cermet [6] and cathode. For stack modeling, this information is too complex, and mostly applies only at low overpotential and current. Furthermore, the results published are valid for the particular materials tested, which usually differ from the ones prepared in-house for electrochemical testing and repeat element assembling [7].

This work intends to present a way of using routine electrochemical results to determine parameters for a kinetic model. This could allow to update a kinetic model following continuous cell development. The usual electrochemical charaterization is simple: a single cell (anode supported electrolyte) with 1 cm^2 cathode is tested at 750 or 800 °C (oven temperature). For the test, a thermocouple is usually placed on the cathode side a few millimeters away from the active area; this temperature rises a little with current (around 4 K at 1.5 A/cm^2). However, there is evidence that the temperature increase on the active surface can reach considerably higher values (around 20–25 °C at 1 A/cm^2 reported [8]).

To use such routine electrochemical testing for a repeat element model, a specific model representing the thermal phenomenon on a single cell has been developed. The temperature versus current and the current–potential characteristics could be reproduced.

2. Methodology

This section presents the method used for calibration of the model developed with the experiments.

2.1. Model and experiment

The experiment carried out differs from the routine electrochemical test. Two thermocouples were employed: one on the usual site (a few millimeters away from the cathode) and one on the cathode itself to monitor the local temperature of the active area.

* Corresponding author. Tel.: +41-21-693-53-57.
E-mail address: diego.larrain@epfl.ch (D. Larrain).

0378-7753/03/$ – see front matter
doi:10.1016/S0378-7753(03)00102-2

The temperature increase on the active surface of the cell is obviously caused by the electrochemical processes taking place on the electrodes. However, the fact that temperature measurement close to that surface is unable to detect this phenomenon is explained by the thermal properties and thermal boundary conditions of the cell. A thermal model describing the reactions, heat transfer and energy balance phenomena has been developed, and is presented in Section 3.

2.2. Parameter estimation: problem formulation

Model and experiments are compared using a parameter estimation method. This methodology is well known in process modeling and is applied here to determine parameters for the thermal model and for the kinetic model. The general formulation for this kind of problem is described here. A model can take the form of a set of equations which must be satisfied:

$$F(\bar{X}, \bar{z}, \bar{\theta}, \tilde{\theta}) = 0 \quad (1)$$

where $\bar{X}$ are the non-measured variables and $\bar{z}$ the measured variables. The set of parameters θ is divided in parameters $\bar{\theta}$ that will be identified by the experiment and $\tilde{\theta}$ which are fixed. The algorithm used is the tool for parameter estimation in the gPROMS [9,10] package and the objective function ϕ to be minimized is the following:

$$\phi = \frac{N}{2}\ln 2\pi + \frac{1}{2}\min_{\theta}\left\{\sum_{i=1}^{\mathrm{NE}}\sum_{j=1}^{\mathrm{NV}_i}\sum_{k=1}^{\mathrm{NM}_{ij}}\left(\ln\sigma_{ijk}^2 + \frac{(\tilde{z}_{ijk} - z_{ijk})^2}{\sigma_{ijk}^2}\right)\right\} \quad (2)$$

where N is the number of measurements; θ the set of parameters to be optimised; NE the number of experiments performed; NV_i the number of variables in the ith experiment; NM_{ij} the number of measurements of the jth variable in the ith experiment; $\tilde{z}_{ijk}$ is the kth measurement value of variable j in experiment i; $\tilde{z}_{ijk}$ is variance of the kth measurement of variable j in experiment i; and z_{ijk} the kth model predicted value of variable j in experiment i.

Experiments with temperature, current and potential measurements are used to calibrate the thermal model (i.e. the temperature response to the current variation). Temperature is measured on the active surface and a few millimeters away from it. The second step is to verify that with a routine electrochemical experiment, values for the kinetics can be found and used with enough confidence.

The difference between measured and predicted values is minimized by the algorithm. Optimization is required due to the non-linearity and complexity of the model which is going to be presented further.

The methodology is based on a two-step optimization. First, experiments with several temperature measurements are made to validate the model and determine the values for some parameters into the thermal model itself. Once those parameters are identified, the tool is ready to be used on the routine electrochemical characterization to determine parameters for the kinetic model.

3. Thermal model

3.1. Experimental set-up and model description

The thermal model intends to represent a cell of small size (16–25 cm^2) with a 1 cm^2 screen-printed cathode (i.e. active area), placed into a seal-less set-up consisting of two spring-loaded flanges with a single gas inlet each. Current collection is achieved by pressing nickel mesh on the anode and platinum grid on the cathode. The cell is kept between two zirconia felts (90% porous). The oven is set to temperature in the range between 650 and 850 °C. Current–potential measurements were recorded with a potentiostat. Two thin thermocouples of 0.1 mm diameter (type K) have been used for the temperature measurements (see Figs. 1 and 2).

As the cell has air and fuel flowing on each side, convective heat transfer takes place. Considering the flanges, heat exchange is mainly due to radiation exchange with the oven's walls. The thermal model represents the following elements:

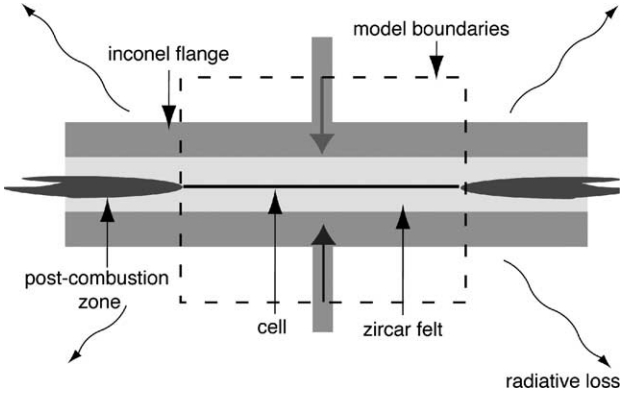

Fig. 1. Seal-less set-up using flanges and zirconia oxide felt to hold the cell in place and feed the gases.

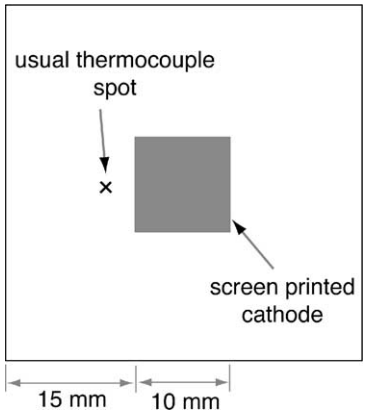

Fig. 2. Scheme of the cell modeled.

- the flanges on air and fuel side;
- the cell (as a single solid layer);
- the gases between the cell and the flanges.

Each of these elements is described with an energy balance equation computing the temperature field. The fuel and oxygen utilization in these tests is inferior to 10% and therefore mass balance equations for the gases are not computed. Introduction of this set of mass balance equations leads to convergence problems because of the discontinuity between the active area and the rest of the cell. Finally the assumptions leading to the energy balance equations are:

- thermal boundary conditions on the flanges are non-adiabatic, the losses are essentially radiative (horizontal mounting limits natural convection);
- a simplified description of the flow pattern in 2D is made with potential flow [11];
- post-combustion of the unreacted hydrogen is assumed to take place at the edge of the cell to the extent of available excess air;
- convective heat transfer is dominating the exchange between solids and gases, the flow is considered laminar and fully developed as first approximation;
- kinetic description is kept simple (ohmic losses and activation term) to be easily handled in a future stack model;
- the temperature gradient in the z-direction of the cell is neglected.

The system boundary of the model is indicated in Fig. 1 and include the end of the gas feed tubes.

The thermal properties for anode supported cells are quite different from those of the electrolyte supported cell where the yttria-stabilized zirconia (YSZ) dominates the heat conduction [12]. The thermal properties of the cermet Ni/YSZ are very sensitive to the composition and porosity. Between 32 and 44 vol.% Ni, and the corresponding porosities, the cell conductivity varies between 4.4 and 10 W/m K. These values are higher than the YSZ thermal conductivity which is usually reported to be on the order of 2 W/(m K).

3.2. Energy balance equations

The different elements of the model are represented by an energy balance equation, this way the temperature field is computed on the whole surface. For the solids (i.e. the cell and the flanges) equations are based on the heat conduction for a 2D plate with source terms:

$$\lambda_{\text{cell}}\left(\frac{\partial^2 T_{\text{solid}}}{\partial x^2}+\frac{\partial^2 T_{\text{solid}}}{\partial y^2}\right)+\sum \dot{Q}=0 \tag{3}$$

where the volumic heat sources $\sum \dot{Q}_{\text{cell}}$ for the cell are the convective terms, the heat of the reaction and the electrical power removed. For the flanges, the heat sources $\sum \dot{Q}_{\text{flange}}$ are the radiative exchange with the oven and the convective exchange with the fluids. The emissivity ϵ_{flange} of the flange is estimated to be in the range of 0.4–0.9 depending on surface state [13].

For the gases, the equations are similar for the fuel and air case. Part of the heat is stored and removed by the gases in the form of enthalpy increase. The heat transfer coefficients h_{air} and h_{fuel} are computed from the Nusselt numbers considering the porous medium of the zirconia felt: this porous flow enhances the heat transfer. The heat transfer regime on the fuel side is dominated by the fuel conduction (hydrogen is much more conductive than the zirconia felt), the Nusselt number is then in the order of 12 [14,15]. On the air side, the Biot number has to be computed first to give a range for the Nusselt number from 40 to 220. The heat transfer coefficients on the air and fuel side are consequently estimated to be 2800–15,500 and 5750 W/m^2 K, respectively. Due to the uncertainty of the first parameter, a sensitivity analysis is useful.

The equations for the gases correspond to the local energy balance of the gas (with a sum on the species i of the mixture). The equation is:

$$\sum_i \mathscr{X}_i \mathscr{C}p_i\left(v_x\frac{\partial T_{\text{gas}}}{\partial x}+v_y\frac{\partial T_{\text{gas}}}{\partial y}\right) = \frac{h_{\text{gas}}}{L}(T_{\text{flange}}-T_{\text{gas}})+\frac{h_{\text{gas}}}{L}(T_{\text{cell}}-T_{\text{gas}}) \tag{4}$$

where $\mathscr{X}i$, $\mathscr{C}p_i$, v_x, L are the molar concentration, the molar heat capacity, the gas-velocity in the direction x computed with the potential flow model and the thickness of the zirconia felt. A boundary condition is imposed at the center of the cell (gas inlet) and is computed with a simple model describing the conduction in the gas feed tube and pre-heating of the gas before reaching the cell. The flow-rates are quite low and in a few centimeters, the gases can heat-up from oven temperature to the gas entry temperature (which is close to the cell temperature at the inlet).

3.3. Sensitivity analysis

Before optimizing the thermal parameters, a sensitivity analysis is necessary. First, if the sensitivity of a parameter is very low, it will be difficult for the algorithm to find an optimum. Second, the size of the problem is reduced. In order to select the parameters of the thermal model to be estimated, the sensitivity analysis was done and the results summarized in Table 1.

From the table, it seems that the thermal conductivity of the cell and the radiative emissivity are the most sensible parameters (considering the response of the active surface temperature T_{act} and the current).

All simulations were done under the same conditions except the changing parameter. They show clearly that optimization has to be performed on the parameters ϵ_{flange} and λ_{cell}. Optimization on the other parameters may lead to problem because of absence of sensitivity. On Fig. 3, the temperature field of a cell operating at 1.5 A/cm^2 is shown. The temperature is maximum on the center were reactions take place and drops with a very steep slope. On the edges,

Table 1
Sensitivity analysis for some thermal parameters, the values gives the variation of the results for each parameter

Parameter	Sensitivity		
	Range	T_{act} (K)	Current (A)
ϵ_{flange}	0.4–1	7	0.1
h_{fuel}	1000–8000 W/(m^2 K)	0	0
h_{air}	2500–15000 W/(m^2 K)	0.5	0.01
λ_{cell}	2–9	2.5	0.05

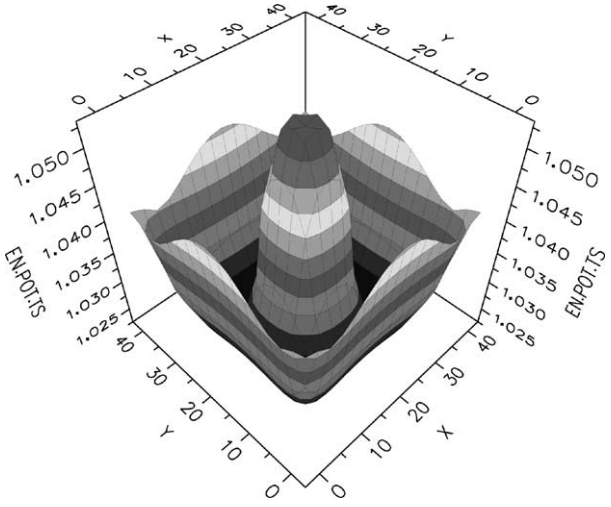

Fig. 3. Temperature profile for the cell at 1.5 A/cm^2.

temperatures are quite high but due to the post-combustion and the low heat conductivity, this is of little importance for the temperature on the active surface.

4. Results and model validation

This section presents the cell tests, results and calibration of the model.

4.1. Cell tests and results

The first set of experimental data is from an anode supported electrolyte (ASE) cell with an $LaSrMnO_3$–YSZ (LSM) composite cathode [16] and the second set with an ASE cell taken from a recent batch with a $LaSrMnO_3$ (LSC) cathode (without cathode firing). The first set of data gave a current density up to 1.2 A/cm^2 whereas our recent state of the art cells [7] deliver up to 2 A/cm^2 current with a LSM–LSC cathode. The new experiment was therefore necessary to measure higher current.

The conditions of the test were flows of 150 and 250 ml/min for hydrogen and air, respectively, the oven was set at constant temperature during each current–potential measurement. As LSC cathode degradation is fast, measurements were done only once. Due to pin-holes on the electrolyte and open circuit voltage (OCV) was only around 980 mV at 700 °C. Nevertheless, power density of 1 W/cm^2 was achieved at 700 °C with current density above 2 A/cm^2.

4.2. Options for an electrochemical model

The first trials used the simplest model considering only an ohmic resistance depending upon temperature. It became rapidly obvious that this option lead to large errors, especially at low current. At low current, activation losses cannot be neglected and a new formulation was tested, taking into account the ohmic losses and activation overpotential. The general electrochemical model gives:

$$U_{Nernst} = \frac{-\Delta G^\circ}{2F} + \frac{RT_s}{2F} \ln\left(\frac{(p_{O_2})^{1/2} p_{H_2}}{p_{H_2O}}\right) \quad (5)$$

$$U_{cell} = U_{Nernst} - R_{ohmic} j - \eta_{act} \quad (6)$$

where, U_{Nernst} is the Nernst potential and η_{act} the activation overpotential. As concentration polarization was never observed even at high current density, that term was neglected. The formulations tested for the activation overpotential were the following:

$$\eta_{act} = -\eta_o(e^{-j/j_p} - 1) \quad (7)$$

$$\eta_{act} = \frac{2RT_{solid}}{n_e F} \sinh^{-1}\left(\frac{j}{2j_o}\right) \quad (8)$$

Eq. (8), equivalent to Butler–Volmer behavior, is applied to both anode and cathode. The exchange current j_o is a function of temperature. The more empirical Eq. (7) gives the activation overpotential as a function of η_o and j_p, which are, respectively, the maximum overpotential and the current density at which the overpotential reaches a plateau. Ohmic losses, η_{act} and j_p are functions of temperature. Both formulations were tested and parameter estimation was run with the experimental data.

4.3. Solution procedure

In a first step, optimization for each temperature is carried out with constant η_o, j_p, R_{ohmic} and the thermal parameters (cell conductivity λ_{cell} and flange emissivity ϵ_{flange}). The gathered results were then used to give an initial guess of the function of temperature for each kinetic parameter (which is a second order polynomial function). Finally, optimization is performed with the complete set of data to adjust the functions. In the end, a continuous function for the kinetic parameters with temperature is obtained. The thermal parameters seem to depend little on temperature [12,13]. This allows to keep them constant on the whole temperature range Fig. 4.

4.4. Results

The model using the simple Butler–Volmer equation could not fit adequately the experimental data. Experimental

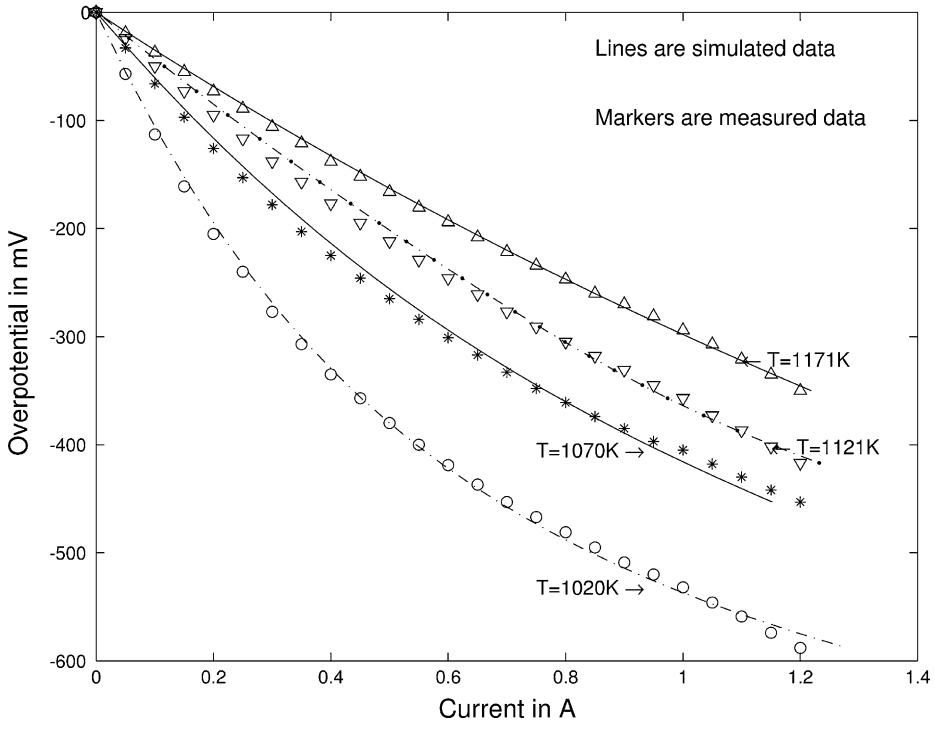

Fig. 4. Current–overpotential relations simulated and measured on an ASE with LSM cathode.

data may be insufficient to determine these parameters, or the model is not complete and therefore is unable to describe the physics. The second model (with Eq. (7)) gives satisfactory fits, Figs. 4 and 5 show the current overpotential characteristics reproduced. The current–temperature response (see Figs. 6 and 7) is also reproduced with reasonable accuracy, though some under evaluation of the temperature remains at high current for the LSM cathode case.

The offset remaining between the experiment and simulated data (see on Fig. 8) on the current–potential

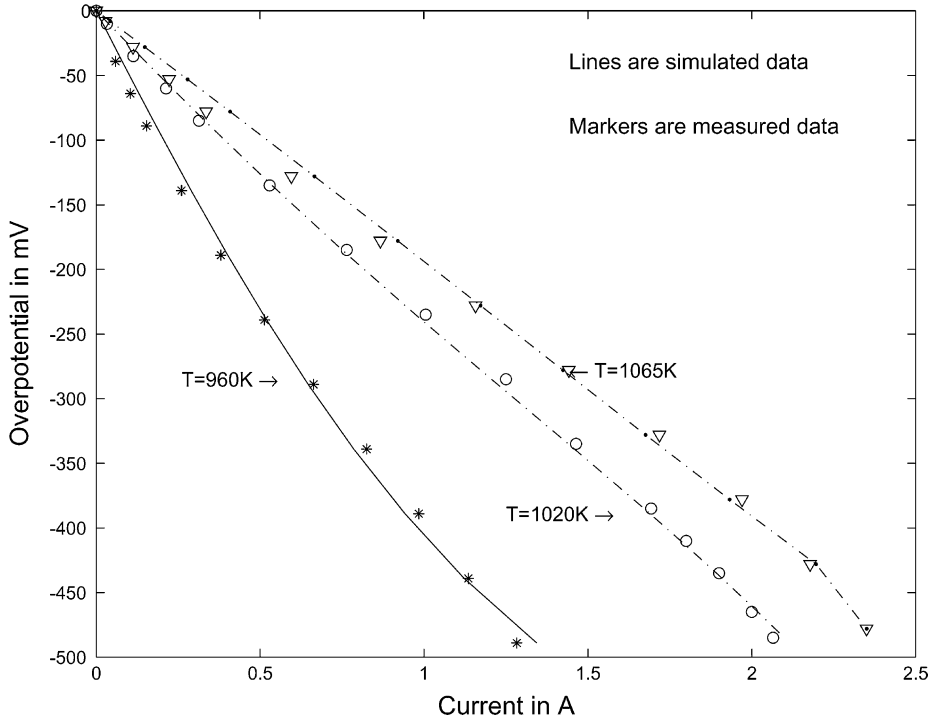

Fig. 5. Current–overpotential characteristics simulated and measured on an ASE with LSC cathode.

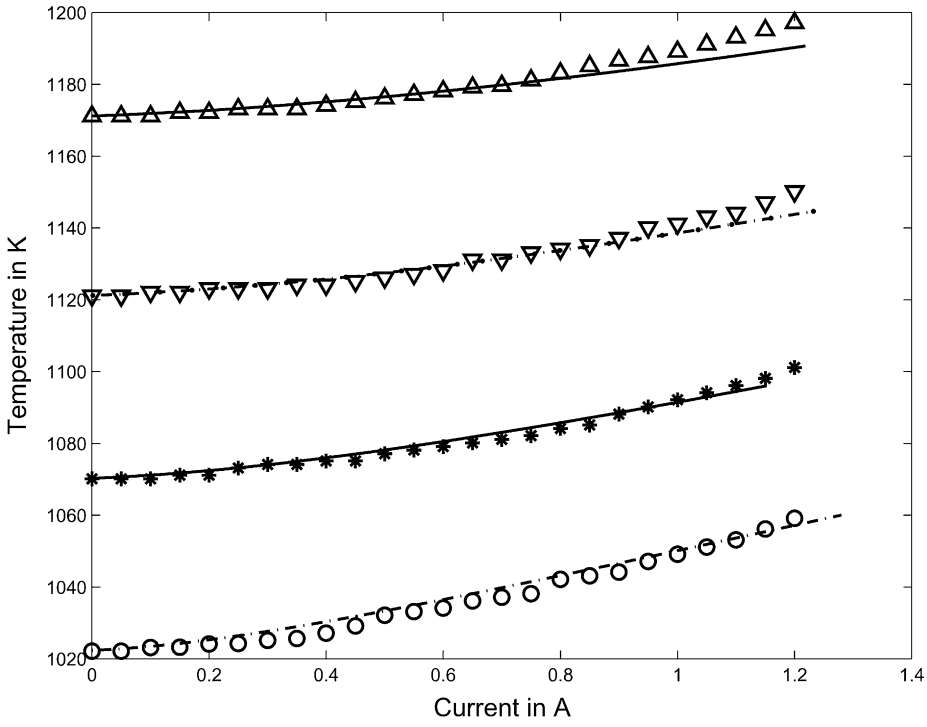

Fig. 6. Temperatures simulated and measured on an ASE with LSM cathode.

characteristics is caused by the difference between the experimental OCV and the simulated OCV, which is on the order of 120 mV. As the data from the current potential measurement was used as an overpotential versus current characteristic for the parameter identification, the OCV was not taken in account. For the temperature response (see Figs. 6 and 7), the differences between simulation and experiments are in the order of 7 K at 1.2 A/cm^2 for the two high temperature measurements in the LSM case. One explanation could be the difference of OCV, that makes the simulation over-estimate the electric power removed from the system.

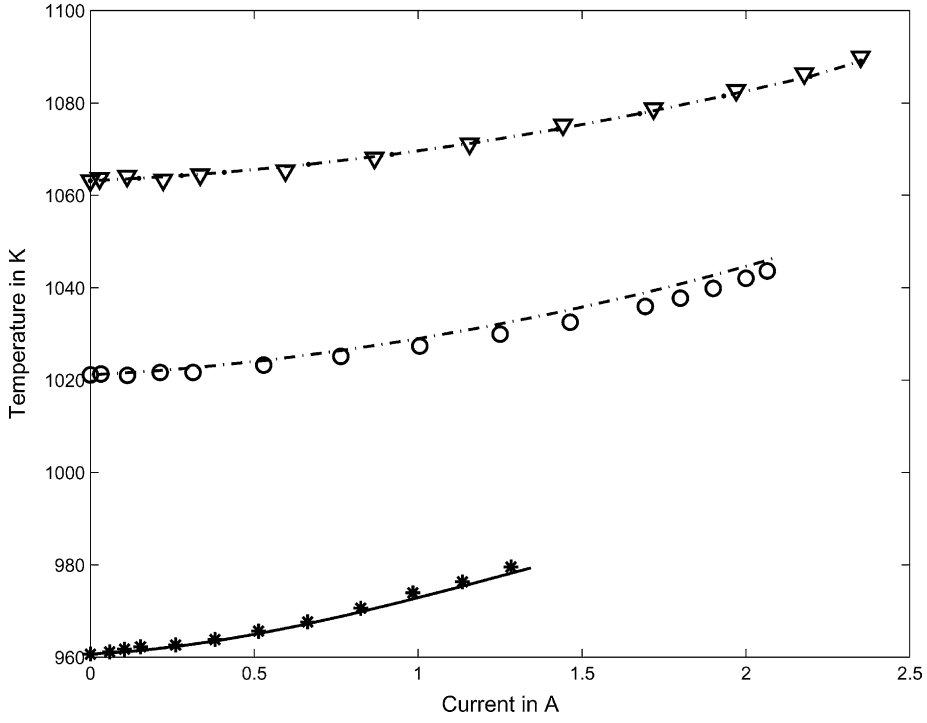

Fig. 7. Temperatures simulated and measured on an ASE with LSC cathode.

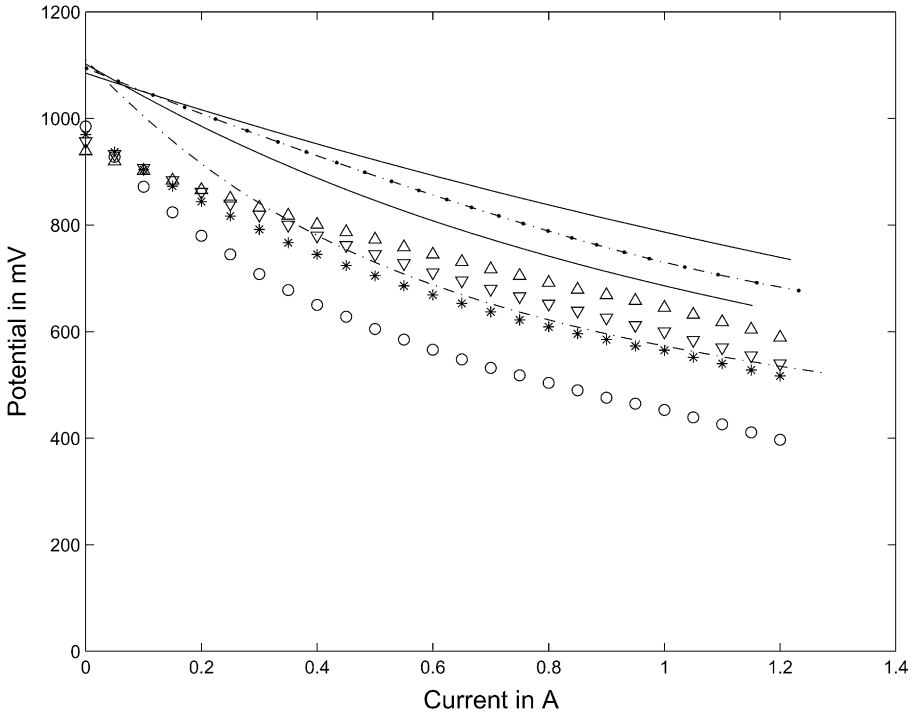

Fig. 8. Current–potential relations simulated and measured on an ASE with LSM cathode.

Table 2
Thermal parameters found for the two cases by the optimization

	λ_{cell} (W/(m K))	ϵ_{flange}
LSM case	7.4	0.36
LSC case	10.1	0.9

4.5. Further work

As the two experiments were not performed in the same set-up, the thermal parameters found for both cases are quite different (see Table 2). To make the routine electrochemical experiment useful, the experiment with two thermocouples in the same set-up and the parameter identification has to be repeated. This will ensure that the thermal parameters λ_{cell} and ϵ_{flange} are constant for this set-up. Once enough confidence on those parameters is obtained, the model can be use to find the kinetic parameters from the routine current-potential measurement.

Regarding the kinetic model, improvements are needed first on the OCV prediction, as simulation over-estimates OCV. An effort should be made in the direction of using an electrochemical model to describe the reaction.

5. Conclusion

A thermal and kinetic model, representing a small solid oxide fuel cell in a set-up used for electrochemical tests has been developed. Using a parameter estimation tool, the simulations have been compared to the experimental results and gave satisfactory fits for both the current–overpotential and temperature–current characteristics. The remaining error is mainly due to the open circuit voltage difference between simulation and experiment. The measurable local increase of temperature on the active area can reach 25–30 K at high current depending on the conditions, as predicted and confirmed by the model. Further experiments should be carried out to allow using the routine electrochemical test for kinetic parameters identification. The kinetic model is now being implemented in a repeat element and stack model which is currently under development.

Acknowledgements

This work was supported by the Swiss Commission for Technology and Innovation (contract 5401.2 SUS). Special thanks are due to Laurent Constantin, Nicolas Badel, Raphael Ihringer and HTceramix SA for the anode supported cells preparation.

References

[1] E. Achenbach, Three-dimensional and time-dependent simulation of a planar solid oxide fuel cell stack, JPS 49 (1994) 333–348.
[2] H. Yakabe, T. Ogiwara, I. Yasuda, M. Hishinuma, Model calculation for planar SOFC focusing on internal stresses, in: Proceedings of the 6th SOFC Conference 99-19, Electrochemical Society, 1999, pp. 1087–1098.
[3] H. Yakabe, T. Ogiwara, M. Hishinuma, I. Yasuda, 3-D model calculation for planar SOFC, JPS 102 (2001) 144–154.

[4] P. Holtappels, I.C. Vinke, L.G.J. de Haart, U. Stimming, Reaction of hydrogen/water mixture on nickel–zirconia cermet electrodes. 1. DC polarization characteristics, JES 146 (5) (1999) 1620–1625.
[5] P. Holtappels, L.G.J. de Haart, U. Stimming, Reaction of hydrogen/water mixture on nickel–zirconia cermet electrodes. 2. AC polarization characteristics, JES 146 (8) (1999) 2976–2982.
[6] B. de Boer, M. Gonzales, H.J.M. Bouwmeester, H. Vermeij, The effect of the presense of fine YSZ particles of porous nickel electrodes, Solid State Ionics 127 (2000) 269–276.
[7] L. Constantin, R. Ihringer, O. Bucheli, J. Van herle, Stability and performance of tape cast anode supported electrolyte (ASE) cells, in: Proceedings of the 5th European SOFC Forum, vol. 21, 2001, pp. 132–139.
[8] J. Van herle, R. Ihringer, R. Vasquez Cavieres, L. Constantin, O. Bucheli, Anode supported solid oxide fuel cells with screen-printed cathodes, J. Eur. Ceram. Soc. 21 (2001) 1855–1859.
[9] M. Oh, C. Pantelides, A modeling and simulation language for combined lumped and distributed parameters systems, Comput. Chem. Eng. 20 (6–7) (1996) 611–633.
[10] gPROMS Advanced User Guide, Process Systems Enterprise Ltd., 2002.
[11] I.L. Ryhming, Dynamique des Fluides, Presses Polytechniques et Universitaires Romandes, 1991.
[12] T. Kawashima, M. Hishinuma, Thermal Properties of porous Ni/YSZ particulate composites at high temperatures, Mater. Trans. JIM 37 (9) (1996) 1518–1524.
[13] F.P. Incropera, D.P. De Witt, Fundamentals of Heat and Mass Transfer, Wiley, New York, 1990.
[14] D.-Y. Lee, K. Vafai, Analytical characterization and conceptual assessment of solid and fluid temperature differentials in porous media, Int. J. Heat Mass Transfer 42 (1999) 423–435.
[15] V.V. Calmidi, R.L. Mahajan, Forced convection in high porosity metal foams, JHT 122 (2000) 557–565.
[16] J. Van herle, J. Sfeir, R. Ihringer, N.M. Sammes, G. Tompsett, K. Kendall, K. Yamada, C. Wen, M. Ihara, T. Kawada, J. Mizusaki, Improved tubular SOFC for quick thermal cycling, in: Proceedings of the 4th European SOFC Forum, 2001, pp. 251–260.